What Does One Learn from Equilibrium Shapes of Two-Dimensional Islands on Surfaces?

Margret Giesen, Christoph Steimer and Harald Ibach

Institut für Grenzflächenforschung und Vakuumphysik, Forschungszentrum Jülich

52425 Jülich, Germany

Abstract

The equilibrium shape of islands has been determined with high accuracy as a function of temperature for Cu(100), Cu(111) and Ag(111)-surfaces. The equilibrium shape is analyzed using the inverse Wulff-construction, the Ising-model, and two novel methods concerning the minimum curvature and the aspect ratio of islands. From the conventional inverse Wulff-construction, the angle dependence of the step free energy is obtained. On Cu(111) and Ag(111), the energies of A- and B-type steps differ only by about 1%. The analysis of the data using the analytical form of the equilibrium shape provided by the Ising-model yields quite acceptable values for the kink energy on (111)-surfaces, but not on the (100)-surface. It is shown that the reason for the failure is due to the different ratio of kink and step energies assumed in the Ising-model for the two surfaces. By combining well-known relations on the statistical mechanics of steps and islands, a simple relation between the kink energy and the minimum curvature of the equilibrium shape is derived and the experimental data are analyzed accordingly for the kink energies on all surfaces. On the Cu(100)-surface, the kink energy compares well with an earlier independent experimental result. The temperature dependence of the free energy of the 100% kinked step in (100)- and (111)-islands is calculated theoretically using general principles. The theory is used to determine the absolute values of the step energies from the experimental data.

1. Introduction

Partly because of their esthetic appeal, partly because of intellectual challenge, researchers have been fascinated by the equilibrium and growth shapes of single crystals for many decades. The large variety of these shapes, as well as their regularity originate from the anisotropy of single crystals, which is directly reflected in the equilibrium shape [1]. Since the surface free energy is a unique function of orientation and temperature, a particular crystal has one and only one equilibrium shape at a given temperature. For many years, studies on the equilibrium shape have been a playground for statistical physics [2-8]. On the experimental side, studies of crystal equilibrium shapes require a complete control of the growth environment as smallest amounts of impurities may have a dramatic effect on the shape. Because of this difficulty, reliable studies on the equilibrium shape became available only relatively recently [9-16]. It is even more recently that we begin to develop an atomistic understanding of the orientation dependence of the free energies as more and more studies focus directly on the atomic aspects of surfaces, be it in the form of first principles total energy calculations or in form of atomically resolved experimental studies employing, e. g., the scanning tunneling microscope (STM).

The surface free energy is determined by the energy of the various crystal facets, the energies of steps and kinks on these facets, and the interaction energy between steps and kinks. Step-step interactions can be studied experimentally by observing the terrace width distribution on vicinal surfaces (see, e. g., [17-20]). The interactions arise from entropic repulsion [4, 21], direct elastic interactions [22], indirect vibrational interactions [23], and possibly electronic interactions [24]. The smallness of the energies involved and the complexity of the interplay [25] between the various contributions makes the analysis of step interactions extremely difficult (see e. g. [20]).

Well established is the determination of the relative facet energies from experimental data on the equilibrium crystal shape [10, 11, 26, 27]. Likewise well established is the experimental determination of kink energies, mostly from studies of (spatial) step equilibrium fluctuations [28-31].

The experimental determination of step energies is less well developed. The dependence of the step free energy on orientation is obtained from the equilibrium shape of two-dimensional islands on surfaces using an inverse Wulff-construction. An elegant method to determine the absolute value of the mean step energy of an island from its equilibrium shape fluctuations was recently proposed by Schlößer et al. [32]. Another method to determine step energies based on the analysis of the three-dimensional equilibrium shape of crystallites [27] still has to face an experimental test.

Equilibrium structures of 2D-islands have been observed by many researchers. Nevertheless, little in terms of quantitative studies is available. In 1994, Bartelt et al. investigated the shape of islands on Si(100) in connection with step fluctuations and derived the step energy and step line tension by making a very clever use of the anisotropy of the Si(100)-surface due to the pairing-row reconstruction [33]. The ratio of the free energies per step length β of the A- and B-type steps on the Pt(111) surface was determined from distances of the corresponding steps to the center of the equilibrium shape by Michely and Comsa [34]. Despite the fact that both step types are oriented along the direction of dense packing (however, displaying a (100)- and a (111)-face, respectively), the ratio of the free energies deviates significantly from 1 (β_A/β_B = 1.15 at 760 K). The same analysis for Cu(111) and Ag(111) as presented here shows hardly any deviation from 1 (see also [35, 36]).

Aside from these, and possibly a few more scattered observations, no systematic analysis of the equilibrium shape of 2D-islands has been reported. It is the purpose of this paper to fill this gap by a detailed experimental study of the equilibrium shape on Cu(100)-, Cu(111)-, Ag(111)-surfaces in a relatively wide temperature range. The data is analyzed, first by using the well-known inverse Wulff-

construction to obtain the orientation dependence of the step free energy. We then proceed to more sophisticated means of analysis by making contact to concepts and results of the statistical mechanics of 2D-objects. We show how to use the minimum curvature of the equilibrium shape (in the orientation of dense packing) to determine the kink energy. Secondly, we show how the absolute value of the step energy for steps along the direction of dense packing (and thus for all other orientations by means of the inverse Wulff-construction) can be determined from a particular aspect ratio of the islands as a function of temperature.

The paper is organized as follows. In the next section, experiments and the procedures for the extraction of the equilibrium shape from the STM images are described. The results are analyzed using the inverse Wulff-construction in section 3. In section 4, we make contact to the Ising-model and discuss the fit of the observed equilibrium shapes to this model. In the two sections to follow, the theoretical background for the further analysis is provided, and the theory is applied to the data to obtain kink and step energies in section 7. The various methods for the analysis of the data and comparison to other methods as well as to theoretical results are discussed in section 8.

2. Experimental

The equilibrium shapes of islands were determined using an STM based on the original design by Besocke and Frohn [37, 38]. Improved thermal and mechanical stability was achieved by using a ceramic base plate for the support of the piezo actuators. The sample temperature was varied by radiation from a filament, electron beam assisted if necessary. The UHV chamber was equipped with an electron beam evaporator (Omicron EFM3) for copper and silver deposition. Special care was taken to degas the evaporator and the Cu/Ag containing crucible so that during deposition the pressure in the chamber never exceeded $1 \cdot 10^{-10}$ mbar. The single crystals used in this experiment

were cut by spark erosion and polished mechanically to an accuracy of 0.1°. Their impurity content was leached by heating in a 1:25 hydrogen and argon atmosphere at 800°C for several hours prior to mounting in the UHV chamber. In order to be able to distinguish between A- and B-steps, the (111)-samples were mounted with reference to the azimuthal orientation as established with the help of Laue diffraction patterns. While for Cu no further treatment is necessary prior to bakeout of the chamber, the Ag crystal was sputtered with Ar^+ for about 2h to remove the ($\cong 10$ μm thick) polycrystalline top layer. After bakeout, the final sample preparation was performed by repeated cycles of sputtering with Ne^+ at 1 kV for 10 minutes (5 μA ion current) with successive annealing of Cu-samples at 700°C and of the Ag-samples at 480 °C for another 20 minutes. After a few cycles, no contamination was detectable in the Auger spectrum. Since the island equilibrium shape is rather sensitive to contamination, a surface coverage below the detection limit of Auger spectroscopy may still have a non-negligible influence on the measurements. We therefore continued the cleaning procedure many cycles beyond the point at which we found the sample clean by Auger standards. In the final cycle before the measurement, the annealing temperature was reduced to 400°C in the case of the Cu-samples to avoid further segregation of bulk impurities (sulfur) onto the surface. The final state of the surface after the preparation procedure was controlled by means of the STM images. After preparation, the observed surface density of pinning sites in the STM images was 10^{-7} per area of an atom. The surface remained clean even after 5-8 hours of observation. The mean terrace width of the surface was 0.5-1 μm before deposition. After the final cycle, the sample was cooled down slowly to the temperature at which Cu and Ag was deposited. The island size and density was controlled by varying the deposition rate between 0.05 and 0.5 ML/s and the temperature of the sample. After deposition, the sample was radiatively heated to the desired temperature and simultaneously mounted to the microscope. The sample was in thermal equilibrium and the tip in a stable tunneling condition for STM recording usually within 5 minutes after deposition. Typical scan

parameters were 1.2 nA, −1.0 V, and a scan speed of 30-60 seconds per 512x512 pixel image. Since no measurable influence on equilibrium step fluctuations was found on Cu(111)- and Ag(111)-surfaces using similar tunneling parameters [39, 40], the tip-surface interactions are negligible in the experiments reported here.

It should be noted that on metal surfaces islands display their equilibrium shape even during epitaxial deposition due to the easier mass transport along step edges compared to the interlayer or intralayer mass transport, provided that the deposition rate is sufficiently low and the temperature sufficiently high. Islands also display their equilibrium shape during coarsening processes. For most of the time, this is even true if the coarsening is due to coalescence. After a coalescence event, the equilibrium shape is quickly re-established via diffusion along the periphery [39, 41].

Examples for the images of islands on the Cu(111)- and Cu(100)-surface are shown in Fig. 1. The figures represent excerpts from the 512x512 original images. The shadows in the image are caused by a high pass filter in the control circuit. The STM images of the islands were analyzed using a special purpose computer code which was implemented as a macro in the image processing software. Starting from a point marked near the center of the island, the program searches along a radial line in a direction θ for the sudden jump in the gray scale values which represent the radial position of the perimeter $r_p(\theta)$. The procedure is repeated for 360 equally distributed angular directions θ. Unphysically large jumps in the radial position of the island perimeter due to occasional noise are filtered out by limiting the difference between the radii corresponding to adjacent values of θ. The island edge positions so obtained are then displayed in the STM image for visual control, a possible change of search parameters and a renewed search.

On the metal surfaces investigated in this study, the island shapes continuously fluctuate due to stochastic noise in the mass flux along the island perimeter. Averaging over large
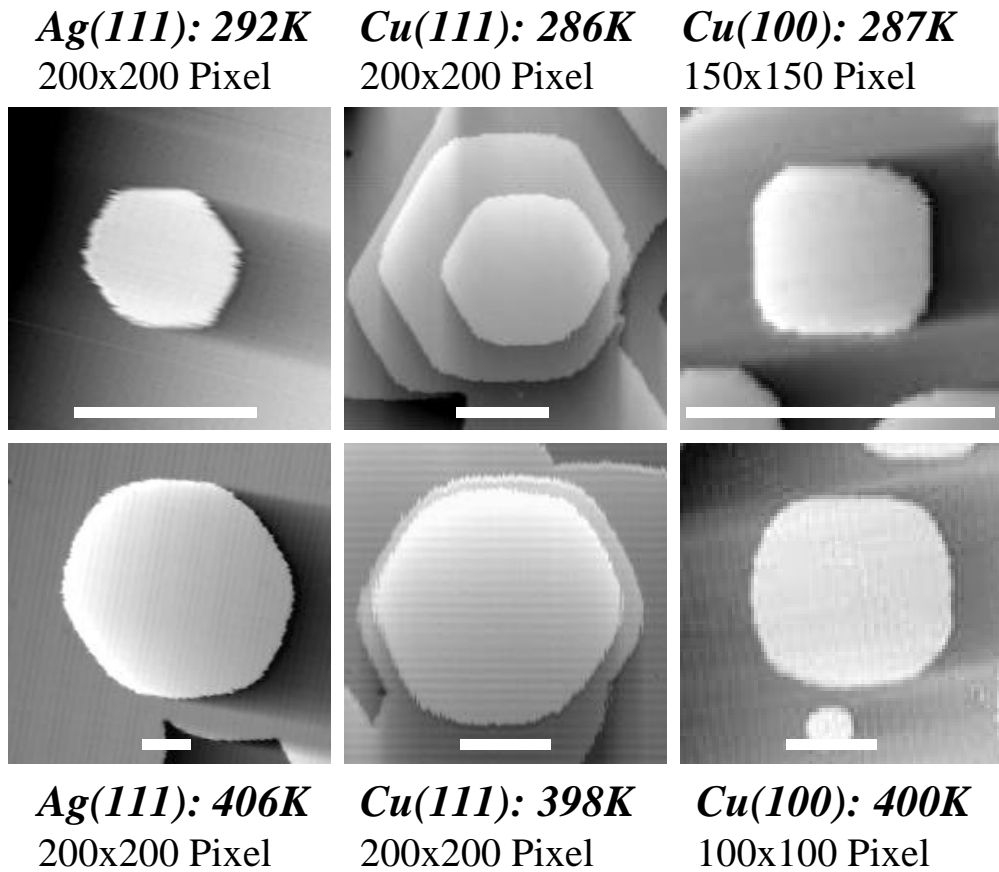
_Ag(111): 292K_   **_Cu(111): 286K_**   **_Cu(100): 287K_**
200x200 Pixel   200x200 Pixel   150x150 Pixel

_Ag(111): 406K_   **_Cu(111): 398K_**   **_Cu(100): 400K_**
200x200 Pixel   200x200 Pixel   100x100 Pixel

Fig. 1:   STM images of islands on the Ag(111), Cu(111)- and Cu(100)-surface at two different temperatures. The images are excerpts from 512×512 pixel images. The white bar in each image corresponds to a length of 20nm. Several hundreds of such images *from several different islands* are averaged to obtain the equilibrium shapes such as displayed in Fig. 2.

ensembles of islands is therefore necessary in order to obtain the equilibrium shape for each temperature. A typical ensemble contained about 100-600 individual shapes, depending on the island size. The individual island shapes in the ensemble were usually picked from several islands in an image and also many images taken at consecutive times. We singled out the few islands which did not fluctuate stochastically in their shape because of pinning centers at the step edge. Since the areas of the different islands are different and also depend, though slowly, on time because of ripening, the shapes were scaled to the same island size prior to averaging. The averaged island shapes were corrected for a small, but nevertheless noticeable distortion of the images due to the anisotropy of the piezo actuators of the STM. The correction involved a general linear transformation (including a

rotation). The matrix elements were determined so that the island shape was optimized with respect to the intrinsic symmetry (C_{4v} and C_{3v} for (100) and (111), respectively).

3. Results and inverse Wulff-construction

As examples for the experimental results two equilibrium shapes of islands on the Cu(100)- and Ag(111)-surface are shown in Fig. 2a and b. The points in Fig. 2 are actual data points and thereby demonstrate the low noise in the data, which is a prerequisite for the quantitative analysis to follow. As expected, the islands appear more cornered at lower temperatures. The shape eventually becomes circular at high T. Island shapes were investigated in the
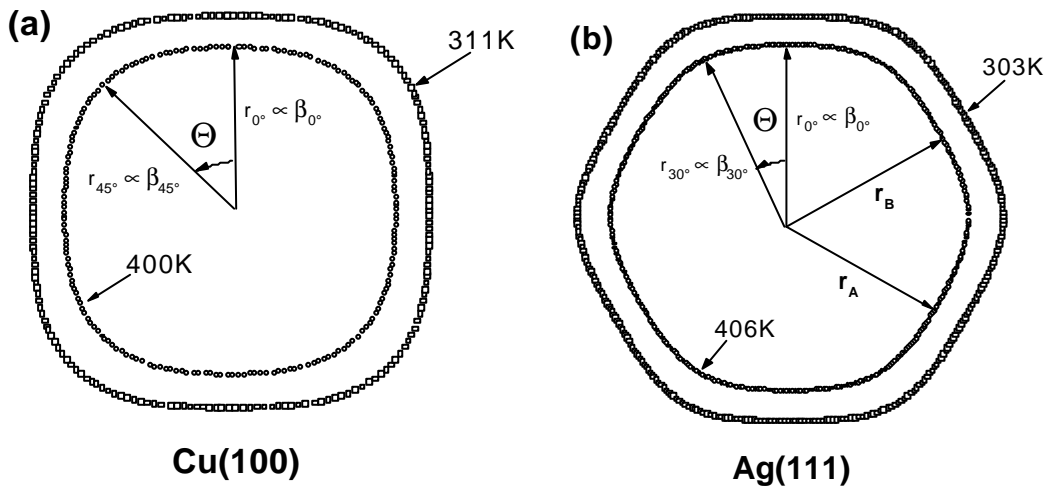

Fig. 2:(a) Two equilibrium shapes for islands on Cu(100) obtained by averaging over 650 and 450 islands, respectively. The radii $r_{0°}$ and $r_{45°}$ are proportional to the free energies $\beta_{0°}$ and $\beta_{45°}$ since the tangents to the shape are perpendicular to the radii in those two cases. The aspect ratio $r_{45°}/r_{0°}$ is therefore equal to the ratio of the free energy $\beta_{45°}$ of the 100% kinked step to the free energy of $\beta_{0°}$ of the step along the densely packed direction. (b) Two equilibrium shapes for islands on Ag(111) obtained by averaging over 104 and 134 (comparatively large) islands, respectively . The radii $r_{0°} = r_A$ and $r_{60°} = r_B$ pointing to the A- and B-steps are proportional to the free energies β_A and β_B. They differ by less than 1%. With the difference in r_A and r_B being that small the length of the radius pointing to $\theta = 30°$ is proportional to $\beta_{30°}$, the free energy of the 100% kinked step.

temperature range of 290K to 450K. The lower limit was because our system was lacking the capability of active cooling. However, the principle limit set by the diffusion along the island perimeter becoming too slow, is about at the same temperature for Cu and not significantly lower for Ag(111). The high temperature limit set by increasing rapidity of coarsening processes. In Fig. 3a-c, equilibrium shapes for Cu(100), Cu(111) and Ag(111) at two different temperatures each are displayed in the form of the radius from the center as a function of the angle θ. The data sets are selected so as to represent the correct mean ratio r_A/r_B and the mean aspect ratio. Here and in the following, the angle $\theta = 0$ refers to the angle at which the perimeter corresponds to the densely packed $\langle 011 \rangle$-direction. For the (111)-surface, $\theta = 0$ denotes the direction where the island perimeter represents an A-step along a $\langle 011 \rangle$-direction. As seen from Fig. 3b and c, the radius $r(0°)$ is larger than the radius $r(60°)$ corresponding to the direction of the B-step on Cu(111), while the inverse is true for Ag(111). The ratio of the radii r_A/r_B is equal to the ratio of the free energies (per length) of the A- and B-steps. Hence, for Cu(111) the A-step has the larger energy. Note that identification of steps as being of the A- or B-type is with reference to the Laue-orientation of the sample. This assumes that the islands grow as to continue the fcc-structure. For Ag(111), Meinel et al. reported that in half the islands the atoms occupy hcp-sites [42]. In that case, A- and B-step reverse the orientation. For Cu(111), Camarero et al. reported that about 20% of the islands are faulted for room temperature deposition and that the ratio rises slowly with temperature [43]. In order to look for stacking faults in our case, we have determined the ratio r_A/r_B from averages over all images of individual islands. We have first looked for a possible temperature dependence of the ratio, however found no statistical significant dependence. The frequency for finding the ratio r_A/r_B in particular ranges are displayed in Fig. 4a and 4b, for Cu(111)and Ag(111), respectively. The presence of faulted islands would give rise to a
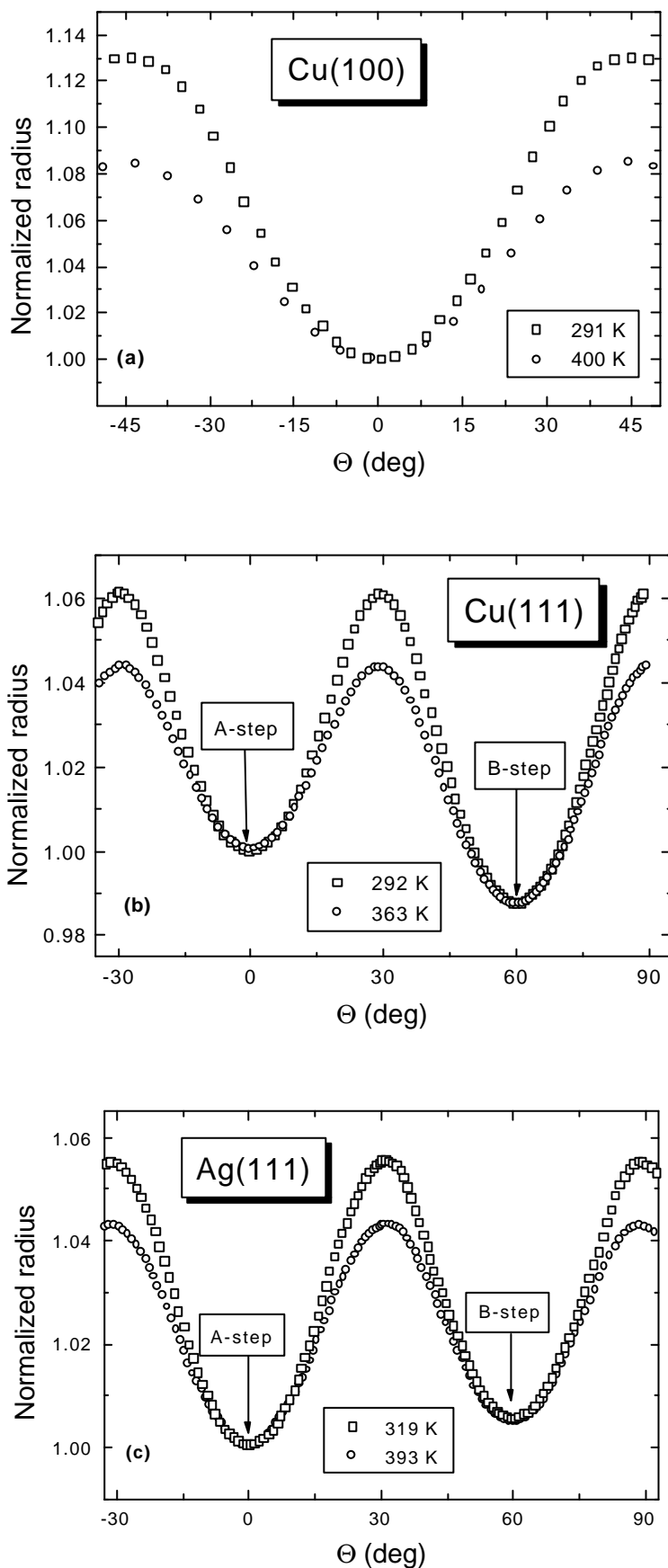
Fig. 3: Normalized radii vs. angle θ for (a) the Cu(100)-, (b) the Cu(111)- and (c) the Ag(111)-surface, respectively.
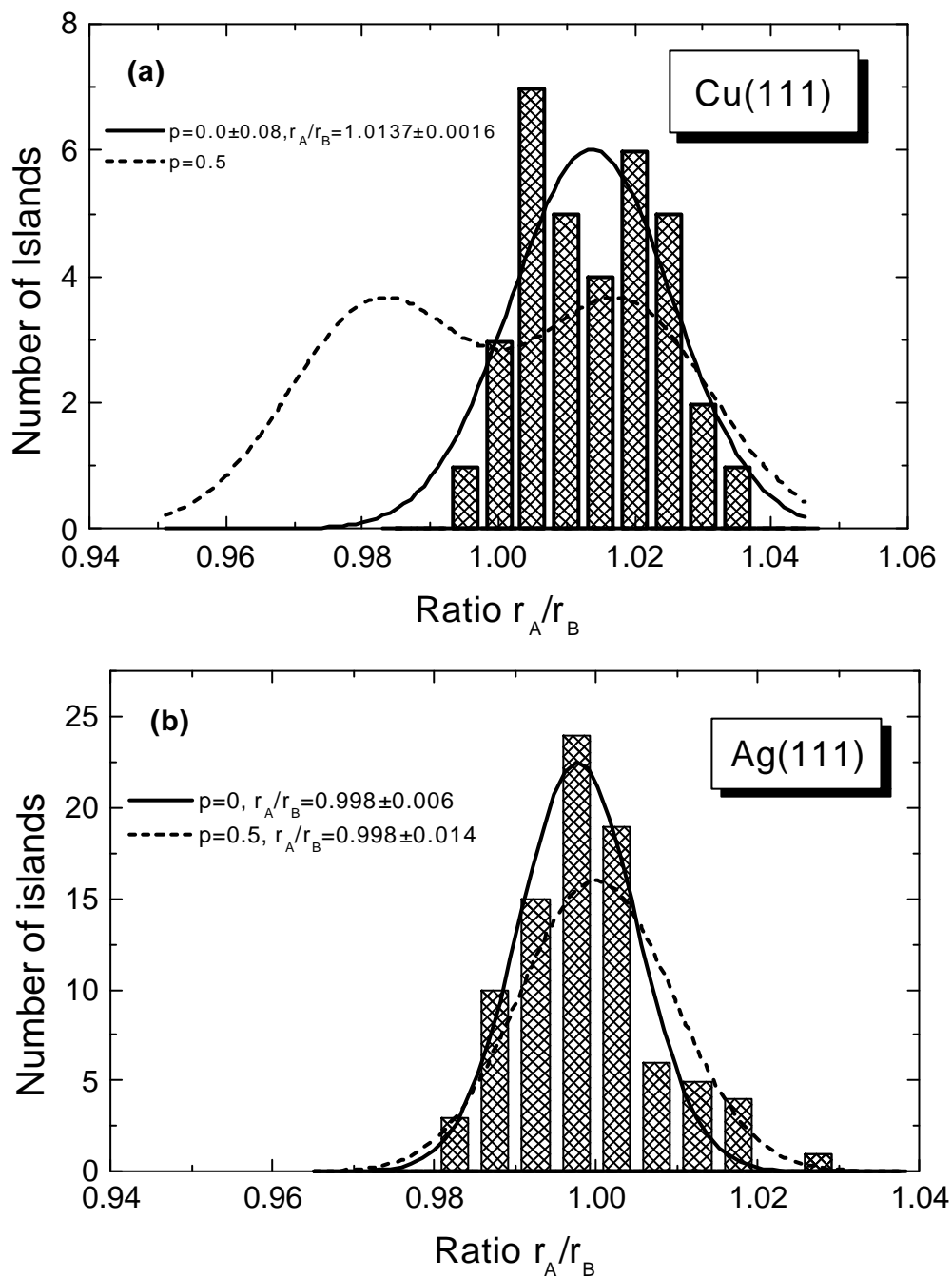
Fig. 4: Histogram for the frequency for finding a particular ratio of radii, (a) for Cu(111) and (b) for Ag(111). The notion A,B here refers to the Laue orientation of the crystal. If islands grow with atoms in hcp position rather than fcc positions the A-steps appear in the orientation of B-steps, and vice versa. Then, the ratio representing the ratio of the free energies of the two kinds of steps would be inversed. For Cu(111) the data exclude an appreciable fraction of faulted islands (see text for further discussion).

double-peaked distribution, centered symmetrically around $r_A/r_B = 1$. This is not observed. In order to analyze the histograms quantitatively we have fitted two gaussians centered at positions placed symmetrically around $r_A/r_B = 1$. Fitted are the position of the centers, the relative weight and a variance parameter. The ratio of the variances of the two gaussians are taken inversely proportional to the square root of the weight, in keeping with the principles of statistics. For Cu(111), the optimum fit is for a zero fraction of faulted islands., $p = 0.0\pm0.08$ (solid line in Fig. 4a). For the purpose of illustration we also show the optimum fit for an assumed fraction $p = 0.5$ as a dashed line. The results show that we do not have a significant fraction of faulted islands in the present experiments. In a previously reported set of experiments in which islands were deposited on some (accidentally wider) terraces of aCu(21 21 23) vicinal surface we found preferentially islands with a ratio $r_A/r_B = 0.989$ which is exactly the inverse of the mean ratio found here [44, 45]. This suggests that faulted islands grow on stepped surfaces, in accordance with the study of Camarero et al [43]. For islands on Ag(111) the fitting procedure described above does not render a significant result on the fraction of faulted islands since the histograms centers practically around $r_A/r_B = 1$. A fit with a fraction of faulted islands $p = 0.5$ fits just as well as $p = 0$ (solid and dashed lines in Fig. 4b, respectively).

By averaging over all results, taking the number of images, the different pixel resolutions, and the number of islands into account we obtain

$$\text{Cu(111):} \quad \beta_A / \beta_B = 1.011 \pm 0.007 \qquad (1)$$

$$\text{Ag(111):} \quad \beta_A / \beta_B = 0.996 \pm 0.0025 \qquad (2)$$

As remarked above, the ratio of the free energies may depend on temperature. However, no significant temperature dependence of the ratio β_A/β_B was observed. A temperature dependence mostly arises from the contribution of step phonons to the free step energy and amounts to a few

meV at 300K [46-48], where the step free energy is a linear function of temperature. The slopes are calculated to be 0.022 and 0.00069 meV/(atom K) for A- and the B-steps, respectively. Since the step energy is about 0.3 eV/atom (see section 5), theory would predict the ratio of the free energies β_A/β_B to vary by about -0.005 for a temperature difference of 100 K. This small variation is not detectable.

In contrast to the ratio β_A/β_B, the ratios of the free energies for the 100% kinked steps (along the $\langle 001 \rangle$- and the $\langle 11\overline{2} \rangle$-directions for the (100)- and the (111)-surface, respectively) to the energies of the densely packed directions depend significantly on the temperature. This is reflected in the ratio of the radii pointing to the "corners" of the islands and the "straight" sections $r_{45°}/r_{0°}$ and $r_{30°}/r_{0°}$, respectively. These ratios are denoted as the aspect ratios of the
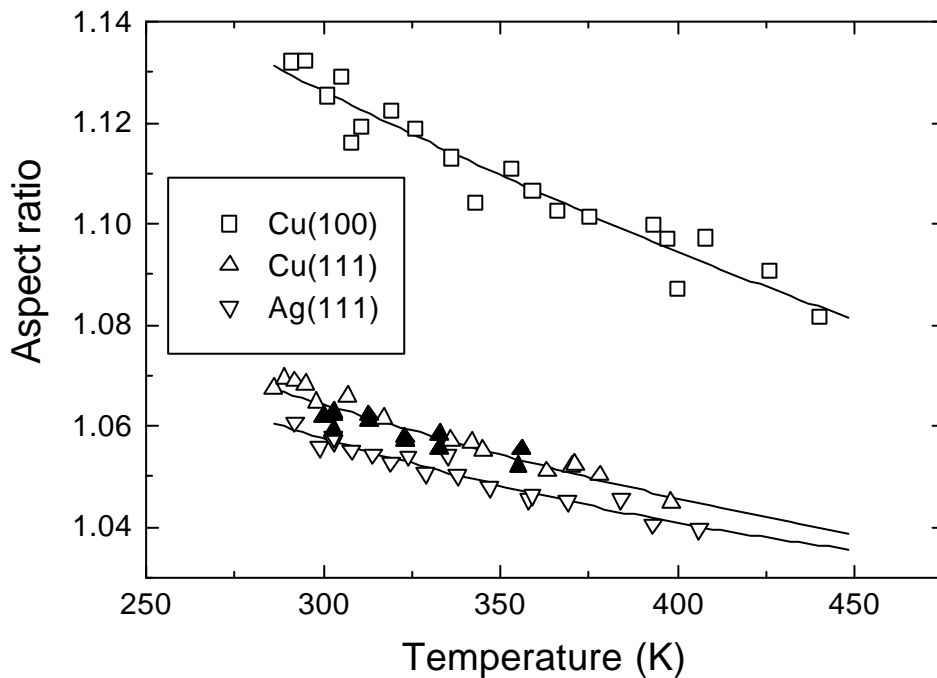

Fig. 5:   Aspect ratio of islands on Cu(100)-, Cu(111)-, and Ag(111)-surfaces as a function of temperature. Data points on Cu(111) include earlier results published in [45] (filled triangles) as well as new results (open triangles). The solid lines are fits to the theory described in sections 6 and 7.

islands in the following. Because of the small difference in the radii of A-steps ($r_{0°}$) and B-steps ($r_{60°}$), we take the average aspect ratio $2r_{30°}/(r_{0°} + r_{60°})$. In Fig. 5, the aspect ratios are plotted vs. temperature for the three types of islands investigated in this paper.

The data for Cu(111) include the data points obtained with islands on (incidentally larger) terraces of vicinal surfaces published earlier in [45] (filled triangles), but extend to lower and higher temperatures. For all surfaces, the ratio decreases monotonically with temperature. The temperature dependence is mostly due to the configurational entropy of kinked steps (section 5).

The dependence of the step free energy on the orientation can be obtained from the equilibrium shape of the islands using an "inverse" Wulff-construction. Two such inverse Wulff-constructions are possible. One, which indeed constructs (the inverse of) the free energy as the minimal surface of the Wulff-construction to the shape of $1/r(\theta)$ [8]. For the two-dimensional case, another form of an inverse Wulff-construction is more convenient as it immediately lends itself to programming a computer code: For a given ray projecting from the origin of the equilibrium shape in the angle θ, one searches for the perpendicular which is a tangent to the equilibrium shape. The distance of the tangent from the origin is proportional to the step free energy. This form of the inversion is possible since two-dimensional islands have no facets for $T > 0$. In other words, the (at low temperatures) seemingly "straight" sections are always curved. The absence of facets in two-dimensional islands means that the step free energy has no cusp in the orientation of dense packing. In Fig. 6a-c, the free energies obtained from the equilibrium shapes are plotted as a function of the angle for Cu(100), Cu(111) and Ag(111) for two temperatures each. Because of the absence of cusps, the lowest term in a power law fit to the free energy function is a term proportional to θ^2. In a reduced form applicable to the plots in Fig. 6, this power law reads
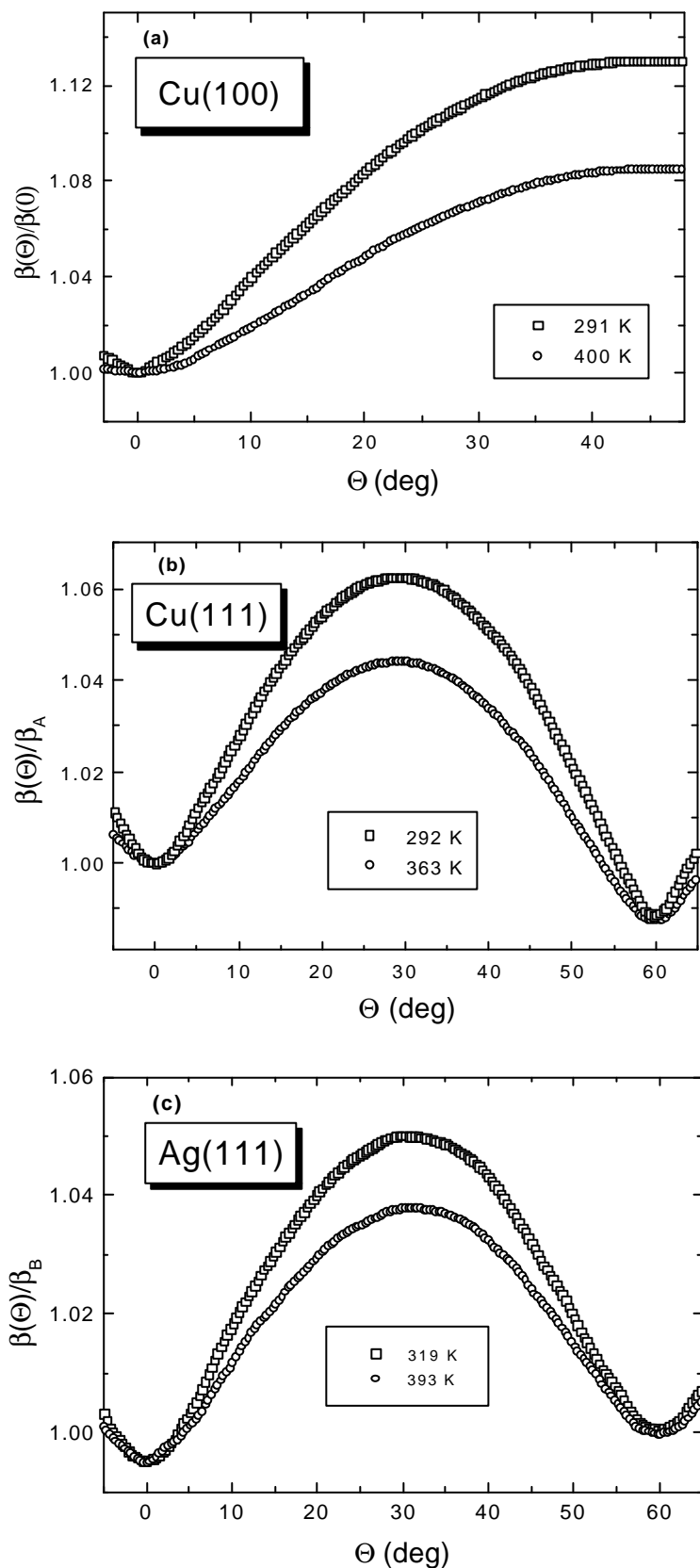
Fig. 6: Variation of the step free energy β as a function of the angle θ for Cu(100), Cu(111), and Ag(111). For the (111)-surfaces, the variation is shown with reference to the step which has the largest free energy. The total variation with the angle reduces as the temperature increases, corresponding to the fact that the islands assume more and more a circular form at higher T.

$$\frac{\beta(\theta)}{\beta(0)} = 1 + \frac{\beta''}{2\beta(0)}\theta^2 + O(\theta^4) . \tag{3}$$

As seen from Fig. 6, the second derivative β'' at $\theta = 0$ decreases with rising temperatures. By referring to a set of well known relations it can be shown that the energy for the formation of kinks in a straight step can be obtained from a suitable Arrhenius type plot of β''. This will be discussed in section 5. Because of the uncertainties introduced by the inverse Wulff-construction, the kink energy is better extracted from the curvature of the equilibrium shape directly (sections 5 and 7).

4. Ising-models

Analytical expressions for the equilibrium shapes of 2D-islands on a square and honeycomb lattice as a function of temperature are available for the Ising-model [3, 49, 50]. In this model, the energy of a step is proportional to its microscopic length. For the square lattice, this means that the energy per atom of the densely packed step and the kink energy are equal. On the honeycomb lattice (henceforth named "hexagonal"), the energy per atom of the densely packed step is twice as large as the kink energy (Fig. 7).
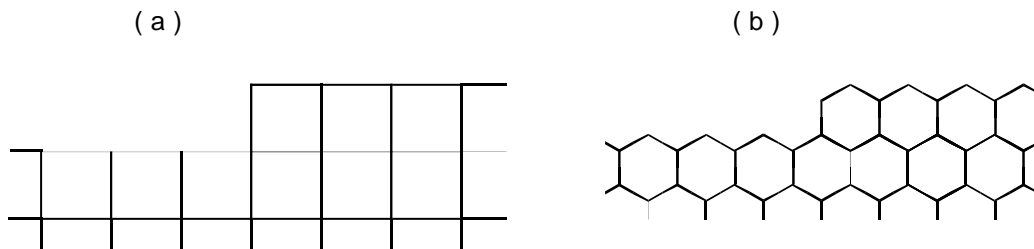

Fig. 7:   Plot to illustrate the energetics in the Ising-model for islands (a) on the (100)-surface and (b) on the (111)-surface. The energies of the steps are proportional to the number of length units. Hence, on the (100)-surface, the kink energy is equal to the step energy per atom whereas on the (111)-surface, the kink energy is half the step energy per atom.

In the following, we denote the energy parameter in the Ising-model which corresponds to the kink

energy as ε. The equilibrium shapes are given by the implicit expressions [3, 49, 50]

$$\cosh\left[\varepsilon(x-y)/2k_BT\right]\cosh\left[\varepsilon(x+y)/2k_BT\right] = A_{sq}, \qquad (4)$$

with

$$A_{sq} = \frac{1}{2}\cosh(\varepsilon/k_BT)\coth(\varepsilon/k_BT) \qquad (5)$$

for the square lattice, and

$$\cosh(2y\varepsilon/k_BT) + \cosh\left((\sqrt{3}x+y)\varepsilon/k_BT\right) + \cosh\left((\sqrt{3}x-y)\varepsilon/k_BT\right) = A_{hex}, \quad (6)$$

with

$$A_{hex} = \frac{\cosh^3(2K^*) + \sinh^3(2K^*)}{\sinh(2K^*)}$$

$$\tanh(K^*) = \exp(-2\varepsilon/k_BT) \qquad (7)$$

for the hexagonal lattice. For moderately low temperatures, i.e., in the limit $\exp(-\varepsilon/k_BT) \ll 1$, the

right-hand sides of eqs. (5) and (7) can be approximated by

$$A_{sq} = \frac{1}{4}e^{\varepsilon/k_BT} \qquad (8)$$

$$A_{hex} = \frac{1}{2}e^{2\varepsilon/k_BT}. \qquad (9)$$

The coordinates are chosen such that for both lattices the nearly straight sections at low temperature

are oriented parallel to the x-axis. The scaling of the cartesian coordinates is so that $y(x=0) = \pm1$ in

the limit $\exp(-\varepsilon/k_BT) \ll 1$, and that the size of the islands described by eqs. (4-9) remains

approximately constant with temperature. In the following, we write down some relations for the

Ising-shapes concerning the radius at $\theta = 0$, i. e. $y(x=0)$, the curvature $y''(x=0)$ and the aspect ratio in a first order approximation in $\exp(-\varepsilon/k_BT)$. The relations represent special forms of general relations, which are considered in sections 5 and 6 in greater detail. The main purpose of the discussion of these relations for the Ising-model is to show to what extent a first order approximation in $\exp(-\varepsilon/k_BT)$ can be used to analyze experimental data. With all terms to first order in $\exp(-\varepsilon/k_BT)$ included, one obtains from eqs. (4)-(7) for $y(x=0)$

$$y_{sq}(x=0) = 1 - \frac{2k_BT}{\varepsilon}e^{-\varepsilon/k_BT} \qquad (10)$$

$$y_{hex}(x=0) = 1 - \frac{k_BT}{\varepsilon}e^{-\varepsilon/k_BT} \qquad (11)$$

These distances of the densely packed, straight sections of the perimeter to the center are proportional to the free energies. [1]

The curvature in the nearly straight sections are

$$y''_{sq}(x=0) \cong \frac{2\varepsilon}{k_BT}e^{-\varepsilon/k_BT} \qquad (12)$$

$$y''_{hex}(x=0) \cong \frac{3\varepsilon}{k_BT}e^{-\varepsilon/k_BT} \qquad (13)$$

Eqs. (10)-(13) depend on the scaling of the coordinates in eqs. (4) and (6). The products

$$yy''\big|_{sq,x=0} k_BT \cong 2\varepsilon e^{-\varepsilon/k_BT}\left(1 - \frac{2k_BT}{\varepsilon}e^{-\varepsilon/k_BT}\right) \cong 2\varepsilon e^{-\varepsilon/k_BT} \qquad (14)$$

---

[1] The free energy per atom $a_{\|}\beta(T)$ of a densely packed step to linear order in $\exp(-\varepsilon/k_BT)$ is $a_{\|}\beta(T) = a_{\|}\beta(T=0) - 2k_BTe^{-\varepsilon/k_BT}$. The factor of two difference in the temperature dependent terms in eq. (10) and (11) is because of the factor of two difference in the step energy for the square and the hexagonal Ising-lattice ($a_{\|}\beta(0)_{sq} = \varepsilon$, $a_{\|}\beta(0)_{hex} = 2\varepsilon$).

$$y y''\big|_{hex,x=0} k_B T \cong 3\varepsilon e^{-\varepsilon/k_B T}\left(1-\frac{k_B T}{\varepsilon}e^{-\varepsilon/k_B T}\right) \cong 3\varepsilon e^{-\varepsilon/k_B T} \qquad (15)$$

are, however, independent of the scaling. The *aspect ratios,* $r_{45°}/r_{0°}$ and $r_{30°}/r_{0°}$, respectively, are

$$\frac{r_{45°}}{r_{0°}} \cong \sqrt{2}\left(1-\frac{\ln 2}{\varepsilon}k_B T\right)\bigg/\left(1-\frac{2k_B T}{\varepsilon}e^{-\varepsilon/k_B T}\right) \qquad (16)$$

$$\frac{r_{30°}}{r_{0°}} \cong \frac{2}{\sqrt{3}}\left(1-\frac{\ln 2}{2\varepsilon}k_B T\right)\bigg/\left(1-\frac{k_B T}{\varepsilon}e^{-\varepsilon/k_B T}\right) \qquad (17)$$

The leading terms for the temperature dependencies are the linear terms in the first parentheses. The

denominators on the right-hand sides of eqs. (16) and (17) are proportional
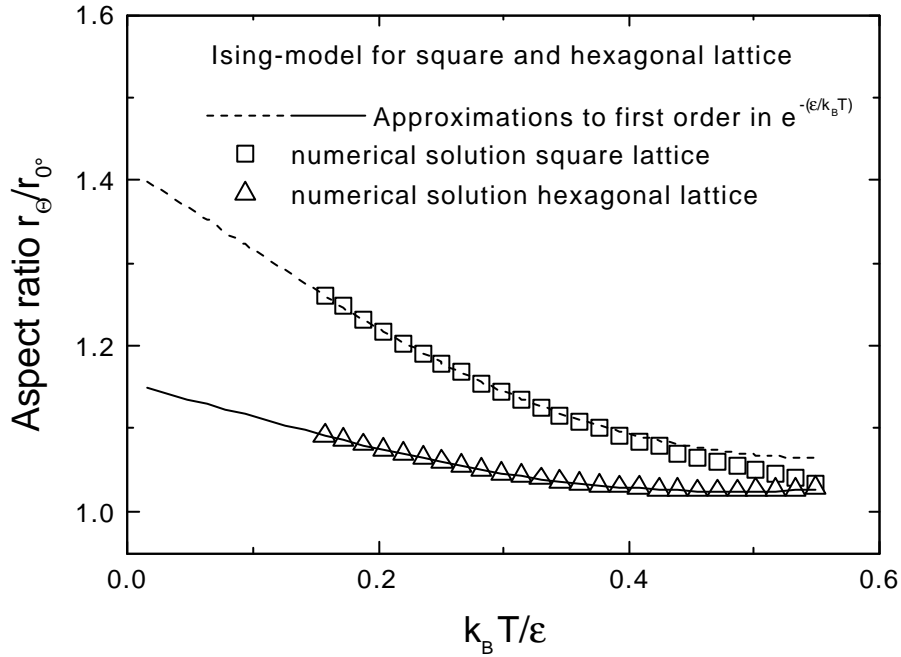

Fig. 8: Comparison of the first order approximation in $\exp(-\varepsilon/k_B T)$ on the aspect ratio to the Ising-model (eqs. (16) and (17)) to the numerically calculated exact Ising result (squares and triangles, respectively). The approximation agrees well with the exact result up to about $k_B T = \varepsilon/2$.

to the free energies of the straight steps. The range of validity of the approximation can be tested by

comparison with the exact (numerical) solution of the Ising-shape (Fig. 8). The approximation agrees

well with the exact result up to $k_B T = 0.4\ \varepsilon$ and $0.5\ \varepsilon$, for the square and hexagonal lattice,

respectively. This condition corresponds to temperatures of 700K, 680K, and 580K for Cu(100), Cu(111) and Ag(111), respectively. Higher order corrections to eqs. (10)-(13) of the order $(\exp(-\varepsilon/k_BT))^2$ can be neglected as long as one uses lower temperatures which is the case, with a good safety margin.

5. Analysis of the minimum curvature

The chemical potential of the curved step of an island in equilibrium is constant along the perimeter by definition. At any point of the perimeter the chemical potential is [51]

$$\mu(\vec{r}) = \Omega \, \widetilde{\beta}(\vec{r}) \, \kappa(\vec{r}), \tag{18}$$

with $\kappa(\vec{r})$ the local curvature and Ω the area per atom; $\widetilde{\beta}(\vec{r})$ is the stiffness of the step describing the work per length necessary to elongate the microscopically meandering step on a coarse grained scale. The stiffness depends on the step orientation θ and is related to the free energy $\beta(\theta)$ (= "line tension") by [52]

$$\widetilde{\beta}(\theta) = \beta(\theta) + \frac{\partial^2 \beta(\theta)}{\partial \theta^2}. \tag{19}$$

The minimum curvature of the perimeter is at $\theta = 0$ ($x = 0$) and eq. (18) becomes there:

$$\mu = a_{\parallel} a_{\perp} \, \widetilde{\beta}(\theta = 0) \, y''(x = 0). \tag{20}$$

The atomic area Ω is expressed now in terms of $a_{\parallel}$ and $a_{\perp}$, the atomic length units parallel and perpendicular to the step oriented along the direction of dense packing (hence, $a_{\perp} = a_{\parallel}$ and $a_{\perp} = \frac{1}{2}\sqrt{3} \, a_{\parallel}$ on the (100)- and (111)- surface, respectively). The chemical potential of an island is

the derivative of the free energy with respect to the number of particles in the island. By using this definition, one derives for the square and the hexagonal lattice at $T = 0$

$$\mu(T = 0) = a_{\parallel} a_{\perp} \frac{\beta(\theta = 0)}{y(x = 0)}. \tag{21}$$

For islands on a (111)-surface with different energies for the A- and B-steps, one obtains the same result with β/y replaced by $\beta_A/y_A = \beta_B/y_B$. In the limit of high temperatures, the islands assume a circular shape and $\tilde{\beta} \equiv \beta$. Relation (21) therefore holds also in the limit of high temperatures since eq. (21) is then identical to eq. (18). Possible temperature corrections in the intermediate temperature range are not known, to the best of our knowledge. We can safely assume that they are at most of the order $\exp(-\varepsilon_k/k_B T)$ and can therefore be neglected around, and moderately above room temperature. Combining eqs. (21) and (20) yields the remarkably simple relation between shape coordinates of islands and energy parameters at $x = 0$, $\theta = 0$.

$$y \, y'' \tilde{\beta} = \beta \tag{22}$$

The stiffness $\tilde{\beta}$ of a step, with a mean orientation along the direction of dense packing ($\theta = 0$), is related to the diffusivity b^2 of a step via (for this and eqs. (24) and (25) see, e. g., [53])

$$\frac{a_{\parallel} k_B T}{b^2} = \tilde{\beta}. \tag{23}$$

The diffusivity of a step is defined by the mean square displacement x of a step

$$g_x(y) = \left\langle \left[x(y) - x(0) \right]^2 \right\rangle = b^2(T) \, y / a_{\parallel}. \tag{24}$$

For not too high temperatures (terms involving $\exp(-2\varepsilon_k/k_B T)$ neglected), the diffusivity can be expressed in terms of the kink energy ε_k as

$$b^2 \cong 2a_\perp^2 e^{-\varepsilon_k / k_B T} \qquad b^2 << a_\perp^2 . \qquad (25)$$

By combining eqs. (22), (23), and (25), one obtains for $x = 0$, $\theta = 0°$:

$$y\, y'' \, k_B T = a_\| \beta \, \frac{2a_\perp^2}{a_\|^2} \, e^{-\varepsilon_k / k_B T} \qquad (26)$$

Eq. (26) offers the interesting possibility to determine the kink energy ε_k from an Arrhenius plot of yy"T. The pre-exponential factor is the step energy per atom, $a_\| \beta(\theta = 0°)$. Eq. (26) is the general form of eqs. (14) and (15) previously derived for the Ising-model, now for arbitrary interactions between the atoms. To the best of our knowledge eq. (26) has not been considered so far, certainly not been used to analyze data. Before we enter the discussion of the experimental results in terms of eq. (26), we mention an alternative way to analyze the experimental data by referring to the inverse Wulff plot. By using eqs. (19), (23), and (25) one obtains

$$1 + \frac{\beta''}{\beta} = \frac{a_\|^2 \, k_B T}{2a_\perp^2 \, (a_\| \beta)} e^{\varepsilon_k / k_B T} . \qquad (27)$$

The ratio β''/β can be obtained from the experimental data with the help of the inverse Wulff-construction (eq. (3)). Again the kink and the step energy can be determined from an Arrhenius plot. Since the use of eq. (27) basically involves the same experimental data on the equilibrium shape, but is subject to errors in the process of the inverse Wulff-construction, the direct analysis of yy"T (eq. (26)) is preferred.

6. Theory of the aspect ratio

The theoretical considerations of this section have partly already been presented in a previous letter publication [45]. Here, we first make contact to the results of the Ising-model and furthermore present and extended discussion of the theoretical implications and a generalization of the theory.

Within the Ising-model, the aspect ratios of square and hexagonal islands are related to the Ising

energy (eq. (16) and (17)). By making reference to the relations between the Ising parameter and the

step energy for one atom length (which is $a_{\parallel}\beta(\theta = 0°, T = 0) = \varepsilon$ for the square lattice, however

$a_{\parallel}\beta(\theta = 0°, T = 0) = 2\varepsilon$ for the hexagonal lattice), one may cast eqs. (16) and (17) into a common

form

$$\frac{r(\theta = \theta_k, T)}{r(\theta = 0, T)} = A(T) \cong \frac{\beta(\theta_k, 0)}{\beta(0,0)} \frac{1 - \dfrac{\ln 2}{a_{\parallel}\beta(0,0)} k_B T}{1 - \dfrac{2k_B T}{a_{\parallel}\beta(0,0)} e^{-\varepsilon/k_B T}} . \tag{28}$$

Here, θ_k denotes the angle of the 100% kinked step. The fact that the aspect ratio of Ising islands

has the same analytical form for the square and the hexagonal lattice raises the interesting question as

to whether the relation also holds for non-Ising systems. In the following, we show that an equation

equivalent to eq. (28) can indeed be derived with an assumption which is far less restrictive than the

assumptions in the Ising-model.

For the Ising-model and also for islands on the (100)-surface the aspect ratio $A(T)$ is equal to the

ratio of the free energies of the 100% kinked step and the step with no structural kinks at $\theta = 0°$.

For islands on the (111)-surface this holds only if the energies for A- and B-steps are equal. For the

moment, we assume that this is so. However, the considerations to follow can easily be generalized

to islands with different energies for A- and B-step. The free energy of the step oriented along the

densely packed direction can be calculated straightforwardly from the partition function per atom

length of this step which is (to second! order in $\exp(-\varepsilon_k/k_B T)$)

$$Z = 1 + 2e^{-\varepsilon_k/k_B T} . \tag{29}$$

The factor of two arises from the possibility to create kinks of opposite sign. The free energy per atom length $a_\parallel \beta(T)$ is therefore

$$a_\parallel \beta(T) = a_\parallel \beta(T=0) - k_B T \ln Z = a_\parallel \beta(T=0)\left(1 - \frac{2k_B T}{a_\parallel \beta(T=0)} e^{-\varepsilon_k/k_B T}\right). \quad (30)$$

With this equation, we have recovered the denominator in eq. (28) which, therefore, has the same form also for general systems. Its temperature dependence arises from the energy
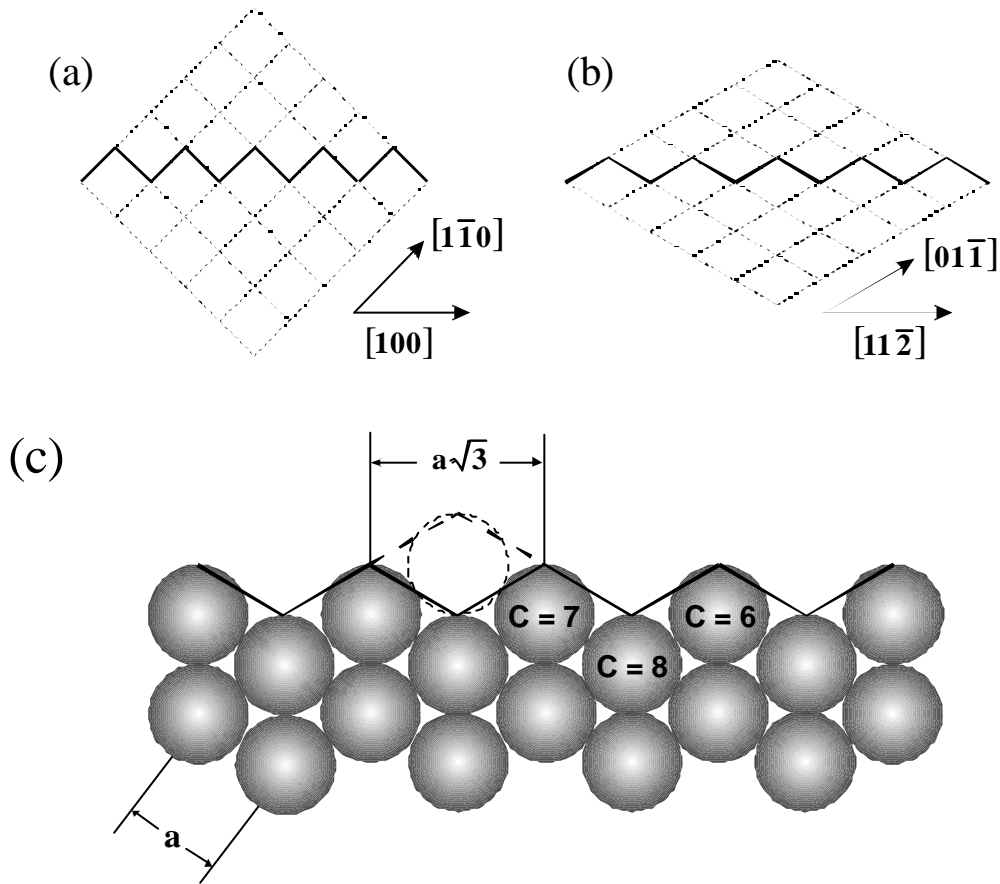

Fig. 9: N=10 length units of the 100% kinked steps (solid lines) for the (a) square lattice and (b) hexagonal lattice. The orientation is along the $\langle 100 \rangle$- and $\langle 11\bar{2} \rangle$-direction, respectively. The ensemble of dashed lines represent paths which have the same microscopic length and therefore nearly the same energy. (c) Structure of a $\langle 11\bar{2} \rangle$-oriented step (solid line) on a (111)-surface. In the macroscopic limit, only configurations which correspond to adding the dashed atom or removing a kink atom from the step contribute to the free energy. Coordination numbers C are indicated for three edge atoms (C=7 is with the added atom).

associated with the creation of kinks in the straight steps. With the energies of the specific step inserted, eq.(30) is valid for A- and B-steps. The linear temperature dependence of the numerator in eq. (28) means that the temperature dependence of the free energy of the 100% kinked step is due to an entropy term. This entropy arises from the various configurations of the steps which all have a mean orientation along the direction of the 100% kinked step and are energetically equivalent in the Ising-model. These various paths are illustrated in Fig. 9a and b, for the square and hexagonal lattice, respectively.

The configurational entropy is calculated easily by making contact with theory [54]: The number of possibilities in a coin tossing game with N trials to arrive at N/2 "head" and N/2 "tale" results is $N!/[(N/2)!]^2$. Thus one has

$$S = k_B \ln \frac{N!}{[(N/2)!]^2} , \qquad (31)$$

which by virtue of Stirling's formula becomes in the macroscopic limit (N→∞)

$$S = N k_B \ln 2 . \qquad (32)$$

Hence, the entropy per atom on the kinked step is $k_B \ln 2$ and the partition function per atom is Z=2. This means that in the macroscopic limit only two alternative paths per atom survive. Those are the ones which stick closest to the center path and correspond to adding or removing one atom to the step as illustrated in Fig. 9c. All other paths have a statistical weight lower then e^N and vanish therefore in the macroscopic limit. With the entropy (eq. (32)), the free energy per atom for the 100% kinked step becomes

$$a_k \beta(\theta_k, T) = a_k \beta(\theta_k, T = 0) - k_B T \ln 2 . \qquad (33)$$

Here, a_k denotes the length per atom of the kinked step which is $a_{\parallel}/\sqrt{2}$ and $a_{\parallel}\sqrt{3}/2$ for the square and hexagonal lattice, respectively. By using eqs. (33) and (30), we calculate for the ratio of the free energies of the 100% kinked step and the "straight" step

$$\frac{a_{\parallel}\beta(\theta_k,T)}{a_{\parallel}\beta(0,T)} = \frac{a_{\parallel}\beta(\theta_k,0) - \dfrac{a_{\parallel}\ln 2}{a_k}k_B T}{a_{\parallel}\beta(0,0)\left(1 - \dfrac{2k_B T}{a_{\parallel}\beta(0,0)}e^{-\varepsilon_k/k_B T}\right)}. \tag{34}$$

This equation is equivalent to eq. (28) since

$$\frac{a_{\parallel}}{a_k} = \frac{\beta(\theta_k,0)}{\beta(0,0)} \tag{35}$$

(cf. also Fig. 7). We now relax the condition which is specific for the Ising-model, namely that the energies of all paths depicted in Fig. 9a,b are equal, and we make allowance for a (small) energy difference ΔE_b between the two paths next to the center path (corresponding to adding or removing one step atom, Fig. 9c). The partition function per atom is then

$$Z = 2\cosh(\Delta E_b/2k_B T) \cong 2\left[1 + \frac{1}{2!}\left(\frac{\Delta E_b}{2k_B T}\right)^2 + \frac{1}{4!}\left(\frac{\Delta E_b}{2k_B T}\right)^4 ...\right]. \tag{36}$$

The additional terms can be ignored as long as $(\Delta E_b/2k_B T)^2 \ll 1$. If that condition is not fulfilled, the absolute value of the partition function is affected by ΔE_b and becomes temperature dependent. Whether or not the partition function of the kinked step is only entropic can therefore be checked by plotting the left-hand side of

$$\frac{a_{\parallel}\beta(\theta_k,T)}{a_{\parallel}\beta(0,T)}\left(1 - \frac{2k_B T}{a_{\parallel}\beta(0,0)}e^{-\varepsilon_k/k_B T}\right) = \frac{\beta(\theta_k,0)}{\beta(0,0)} - \frac{a_{\parallel}\ln Z(T)}{a_k\,a_{\parallel}\beta(0,0)}k_B T \tag{37}$$

vs. temperature. The deviation from a straight line is then due to the temperature dependence of the partition function. The three unknown parameters in eq. (37), which are $\beta(0,0)$, ΔE_b, and the ratio $\beta(\theta_k,0)/\beta(0,0)$, can be determined from a self consistent fit of the temperature dependence of the experimental ratio of the free energies $\beta(\theta_k,T)/\beta(0,T)$. This fit requires that the data have a sufficient low noise and extend over a sufficiently wide temperature range.

7. Analysis of the experimental data

7.1 Finite size effects

The Ising-model as well as the more general theory for the aspect ratio presented in the preceding section refer to the island shape in the macroscopic limit. For a meaningful theoretical analysis of experimental equilibrium shapes of islands, one needs to know beyond which size it is legitimate to assume that errors due to the finite size of the islands are small. We address the issue from two sides, (i) by measuring the aspect ratio of islands as a function of size and, (ii) by estimating finite size corrections to eq. (32). Different island sizes were obtained by depositing material at different rates and sample temperatures. Islands sizes differing by about three orders of magnitude in area were thereby obtained. However, the smallest islands preferentially obtained at low temperatures cannot be measured at high temperatures since they decay too quickly. For a given temperature we have therefore only a range of about 25 in area, respectively 5 in the linear dimension available. As an example, the aspect ratio of islands on the Ag(111)-surface is plotted versus the island radius $r_{30°}$ in Fig. 10a. The error bars in Fig. 10a are estimated from the pixel resolution and the number of islands in the ensemble. As this latter number varies considerably, the error bars differ for each lot and are larger for the smaller data sets on small islands. In Fig. 10b the aspect ratio of islands is plotted versus the full range of sizes investigated which ranges from 500 to
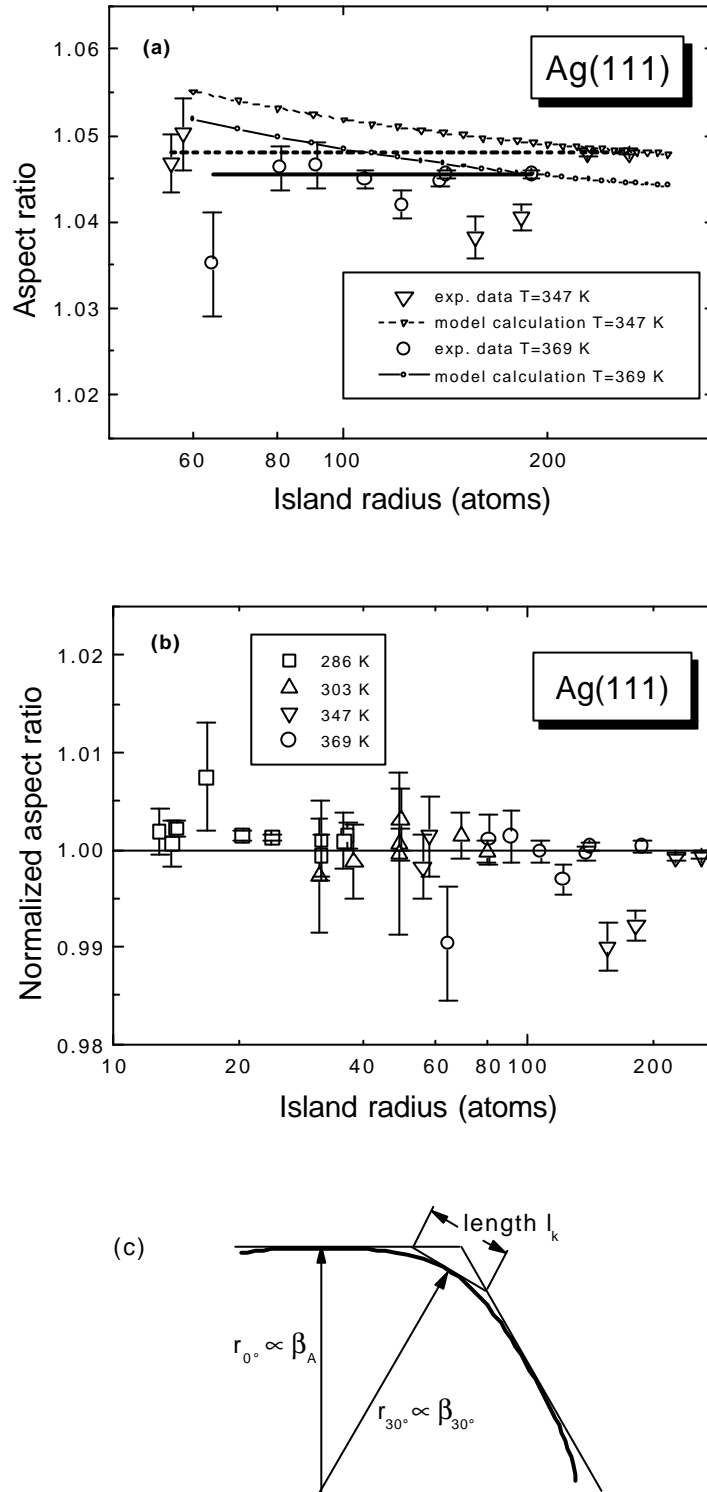
Fig. 10:(a) Aspect ratio of islands vs. the radius $r_{30°}$ for Ag(111) for two different temperatures (large triangles and circles). The thick dashed and solid lines represent the mean values of the aspect ratio. The thin dashed and solid lines connecting the small symbols are a simple estimate for the finite size effect in the aspect ratio as described in the text. (b) Aspect ratio of islands in a wider range of sizes normalized to the mean aspect ratio obtained for large islands (full curve in Fig. 5). (c) Sketch to illustrate the length l_k of the 100% kinked step (see text).

200 000 atoms (a factor of 20 in radius). In order to be able to compare measurements at different temperatures the aspect ratios are normalized to the mean aspect ratio (full line in Fig. 5). The data in Fig. 5 were always obtained with largest islands at a given temperature. A finite size effect would therefore be apparent in Fig. 10b by a deviation of the aspect ratio for the smaller islands for each temperature. The data display no finite size effect, not even in the set obtained at 286 K with radii between 12 and 37 atoms (open squares in Fig. 10b). This result came somewhat unexpected to us as it is at variance with a simple model that one may consider for a theoretical estimate on the finite size effect.

The assumption that the island size be large is explicitly made with the use of the Stirling approximation for eq. (31), and it is presumably there where the assumption of infinite size should enter most significantly. For islands of finite size, the number of atoms in the 100% kinked step denoted as N is no longer infinite and the partition function per step atom becomes smaller for small islands, and the aspect ratio becomes larger. If one denotes the change in the partition function due to the finite size as $\Delta Z(r)$, with $\Delta Z(r)$ being a yet to be determined function of the island radius, the change in the aspect ratio is approximately (eq. (34))

$$\Delta(r(\theta_k)/r(0°)) \cong -\frac{a_\parallel}{a_k}\frac{\Delta Z(r)\,k_BT}{a_\parallel\beta(0°,0)}. \tag{38}$$

The relation between the change in the partition function and the size of the islands is estimated in the following way: The tangent to the 100% kinked step intersects the shape of an ideal hexagon after a length $l_k = 2r_{0°}(1-r_{30°}\sqrt{3}/2r_{0°})$ (Fig. 10c). We assume that a reasonable value for the number of atoms in the 100% kinked step N is given by the length of that tangent, $N = 2l_k/a_k$. $\Delta Z(r)$ is then calculated from the difference between the partition function for $N = 2l_k/a_k$ and $N = \infty$. The finite size corrections according to that model are plotted in Fig. 10a as the small open and filled triangles

connected by a thin dashed and solid line, for the two temperatures respectively. Comparison to the experimental data suggests that the model overestimates the finite size effect grossly. Recent Monte-Carlo calculations support this view [55]. In summary, we conclude that for the purpose of the present study finite size effects can safely be neglected for islands containing more than about 5000 atoms. For a more precise determination of the effect of finite island sizes on the aspect ratio and other feature of the equilibrium shape, a detailed comparison of experimental data to Monte-Carlo simulations would be required, which is beyond the scope of the present paper.

7.2 Analysis using the Ising shapes

A comparison between the Ising-model and experimental equilibrium shapes can be performed in several ways. The most straightforward way is a least square fit to the overall shape with the Ising energy ε as the free parameter. An example to illustrate the quality of such fits is shown in Fig. 11. The squares represent experimental data on the equilibrium shape of Cu(100) islands at 400K. The full line is the least square fit of the Ising-shape with the optimum value for the parameter $\varepsilon = 0.086$ eV. The agreement is remarkably good. Nevertheless, the value of the parameter ε such obtained agrees neither with the kink energy, which is $\varepsilon_k = 0.128$ eV [30], nor with the step energy, which is $a_{\parallel}\beta(0) \cong 0.22$eV (this work). The Ising-shape calculated with the experimentally known kink energy $\varepsilon = \varepsilon_k = 0.128$ eV, on the other hand, deviates dramatically from the measured equilibrium shape (dashed line in Fig. 11). The main reason that ε is lower than both the kink and the step energy is that in the Ising-model, the ratios of the energies for the 100% kinked step and the straight step, and therefore the aspect ratios at T = 0, are fixed to $\sqrt{2}$ and $2/\sqrt{3}$, for the square and hexagonal
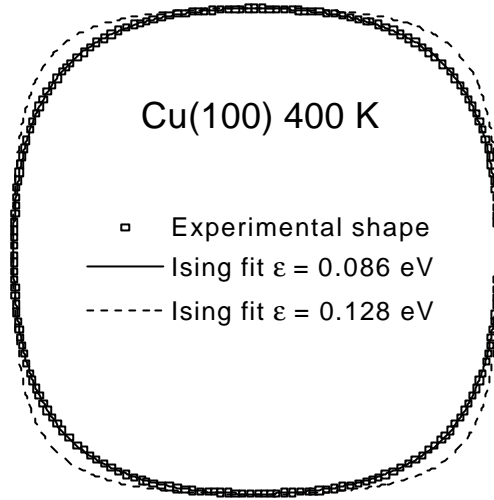
Fig. 11: Comparison of the experimental equilibrium shape (circles) of Cu(100) at 400K to the Ising-model. The best fit (full line) is obtained with ε of 0.086 eV. Despite the good overall fit, the Ising energy ε does not at all agree with the kink energy $\varepsilon_k = 0.128$ eV. The Ising shape with $\varepsilon = \varepsilon_k$ (dashed line) on the other hand, does not at all agree with experiment. Neither the kink energy ε_k nor the step energy $a_{\parallel}\beta$ can be extracted from a fit to the Ising-model. See text for further discussion.

lattice respectively. In reality, the ratios may differ significantly from these numbers. For the Cu(100)-surface, the ratio $\beta_{45°} / \beta_{0°}$ is much smaller than $\sqrt{2}$ (Fig. 5, see also section 7.3). The least square overall fit of an Ising-shape to the experimental data is most sensitive to the aspect ratio and less sensitive to the curvature at $x = 0$ which is directly related to the kink energy (eq. (26)). In the Ising-model, the only possibility to bring down the aspect ratio to the lower experimental value is via the linear term in T in eq. (16) by choosing a low value for ε, and hence, low values for ε are obtained by fitting with the Ising-model. In Fig. 12 the Ising-parameters obtained by fitting island shapes at various temperatures to the Ising-model are displayed as a function of temperature The failure of the Ising-model is also apparent from the temperature dependence of the Ising-parameter. For the (111)-surfaces of Cu and Ag the Ising-model works better: there, the mean value of the Ising parameter ε is close to the kink energy ε_k, as determined from an Arrhenius plot of the curvature (Figs. 12b, c). As far as one can tell from the data, the Ising-parameter remains to be temperature dependent.
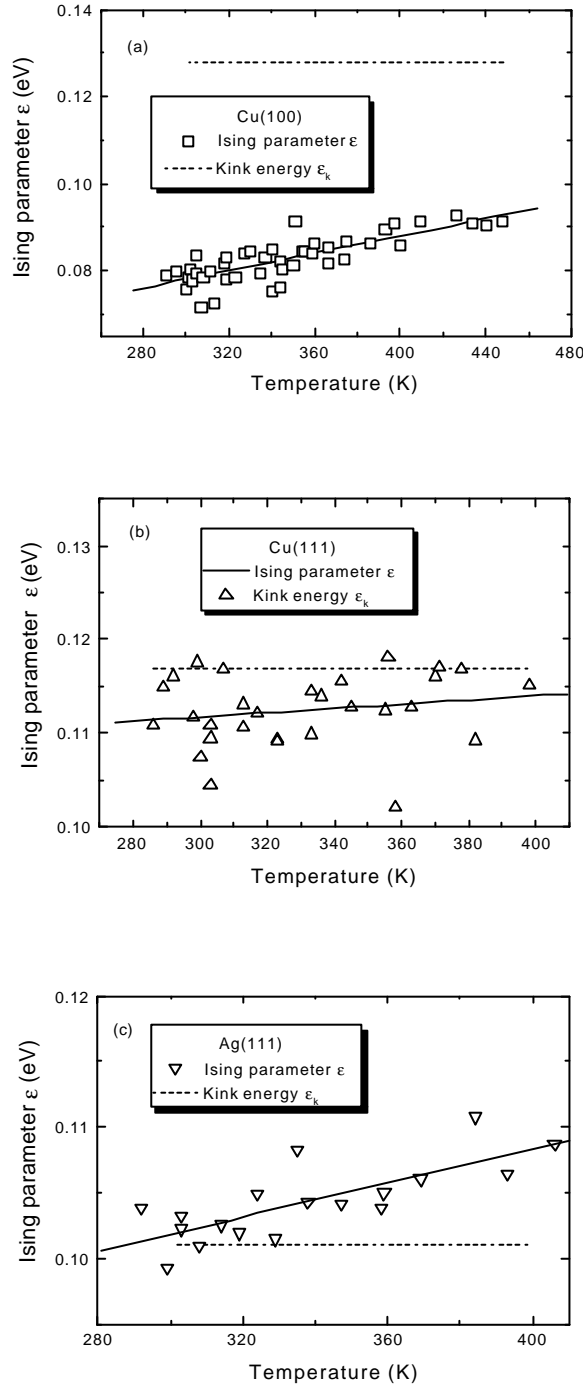
Fig. 12: Ising-parameter ε obtained from a least square fit to experimental equilibrium shapes of (a) Cu(100)-, (b) Cu(111)- and (c) Ag(111)-islands. The dashed line represents the kink energy ε_k. In the case of the Cu(100)-surface, the value is obtained from the step position correlation function (ε_k=0.128±0.003 eV [30]). For the Cu(111) and the Ag(111)-surface, the numbers are 0.117±0.006eV and 0.101±0.005eV, respectively, and are obtained from the analysis of the curvature vs. temperature described in sections 5 and 7. For Cu(100), the Ising-parameter deviates significantly from the kink energy, because the experimental aspect ratio is not well represented by the Ising-model. For the (111)-surfaces, the Ising-parameter agrees reasonably well with the kink energy ε_k. *However, the Ising-parameter remains to be temperature dependent, as in the case of Cu(100).*

7.3 The minimum curvature

According to eq. (26), the minimum curvature in the nearly straight section, respectively the second derivative y" of the equilibrium shape at $\theta = 0°$, can be used to determine the kink energy from an Arrhenius plot of y($\theta = 0$) y"($\theta = 0°$) T. The second derivative was determined by fitting a parabola centered at $\theta = 0°$ (equivalent to x = 0) to the experimental data using a finite range of $\theta -$ values. We have analyzed the minimum curvature of the experimental island shape data employing fitting ranges $\Delta\theta$ between $\pm 8°$ and $\pm 20°$. Examples for $\Delta\theta = \pm 10°$ are shown in Fig. 13a-c for Cu(100), Cu(111), and Ag(111), respectively.

Surface	Fitting range $\Delta\theta$	Slope (eV)
Cu(100)	±8°	0.1266±0.015
Cu(100)	±9°	0.1400±0.017
Cu(100)	±10°	0.1285±0.013
Cu(100)	±15°	0.1014±0.006
Cu(111)	±9°	0.1187±0.013
Cu(111)	±10°	0.1106±0.011
Cu(111)	±12.5°	0.1082±0.005
Cu(111)	±15°	0.1007±0.006
Ag(111)	±9°	0.0984±0.009
Ag(111)	±10°	0.0991±0.007
Ag(111)	±12.5°	0.0944±0.007
Ag(111)	±15°	0.0898±0.005

Table 1: Slopes of Arrhenius plots of ln(yy"T) according to eq. (26), with y" obtained from fitting a parabola to the equilibrium shape around the position of minimum curvature. For the (111)-surfaces the mean value of the step energy for A and B-steps is used.

For the (111)-islands, the data represent an average over A- and B-steps. The slopes of the Arrhenius plots are listed in Table 1. While, for obvious reasons, the error decreases for larger fitting ranges $\Delta\theta$, there is also a trend towards smaller slopes for larger $\Delta\theta$. This is because fitting a parabola to data in a finite range of angles overestimates the true curvature at $\theta = 0$. The error is the larger, the lower the temperature is. As a consequence, fitting to data points in too large a $\theta-$range

results in a lower slope of ln(yy''T), and thus, in a lower apparent kink energy. In order to minimize the error introduced by the finite $\Delta\theta$ we have used only slopes from fitting ranges up to 12.5°. In Table 2 the mean values of the kink energies obtained for the fitting ranges $\Delta\theta = 8°$, 9°, and 10° and $\Delta\theta = 9°$, 10°, and 12.5° are listed for Cu(100), Cu(111) and Ag(111), respectively. To estimate the remaining effect of the finite angular fitting range, we have analyzed square and hexagonal Ising shapes the same way as the experimental data.

Surface	ε_k (eV)	ε_k(corr.)
Cu(100)	0.131±0.009	0.129±0.009
Cu(111)	0.112±0.006	0.117±0.006
Ag(111)	0.097±0.005	0.101±0.005

Table 2: Kink energies ε_k obtained from the Arrhenius plots of yy''T. Data in the first column represent the mean obtained for the fitting ranges between ±8° and ±12.5°. The values are corrected for the finite angular fitting range according to the Ising-model (see text). For the (111)-surfaces, the kink energies represent mean values for A- and B-steps. The differences in the kink energies for the A- and B-steps are small but noticeable in the case of Cu(111) (see Fig. 14).

The temperature range was 290K to 420 K. To represent the island shapes approximately, the Ising energy was chosen as 0.11 eV. With this result from the Ising-model, the experimental data obtained with the finite fitting ranges were extrapolated to $\Delta\theta = 0°$. The result of this extrapolation is displayed in the third column of Table 2 as ε_k(corr).

So far, the analysis assumed that the kink energies for A- and B-steps were equal. The curvatures plotted in Fig. 13 b and c are averages over A- and B-steps. The kink energies in Table 2 therefore represent the mean kink energies for A- and B-steps. In addition to the mean value, one can also determine the ratio of the kink energies. For this purpose, eq. (26) is written for A- and B-steps independently and the ratio of the kink energies is then determined from the individual curvatures for A- and B-steps according to

$$\frac{\varepsilon_k(A-step)}{\varepsilon_k(B-step)} = \frac{\ln(2y_A y_A'' kT / 3a_\parallel \beta_A)}{\ln(2y_B y_B'' kT / 3a_\parallel \beta_B)}. \tag{39}$$
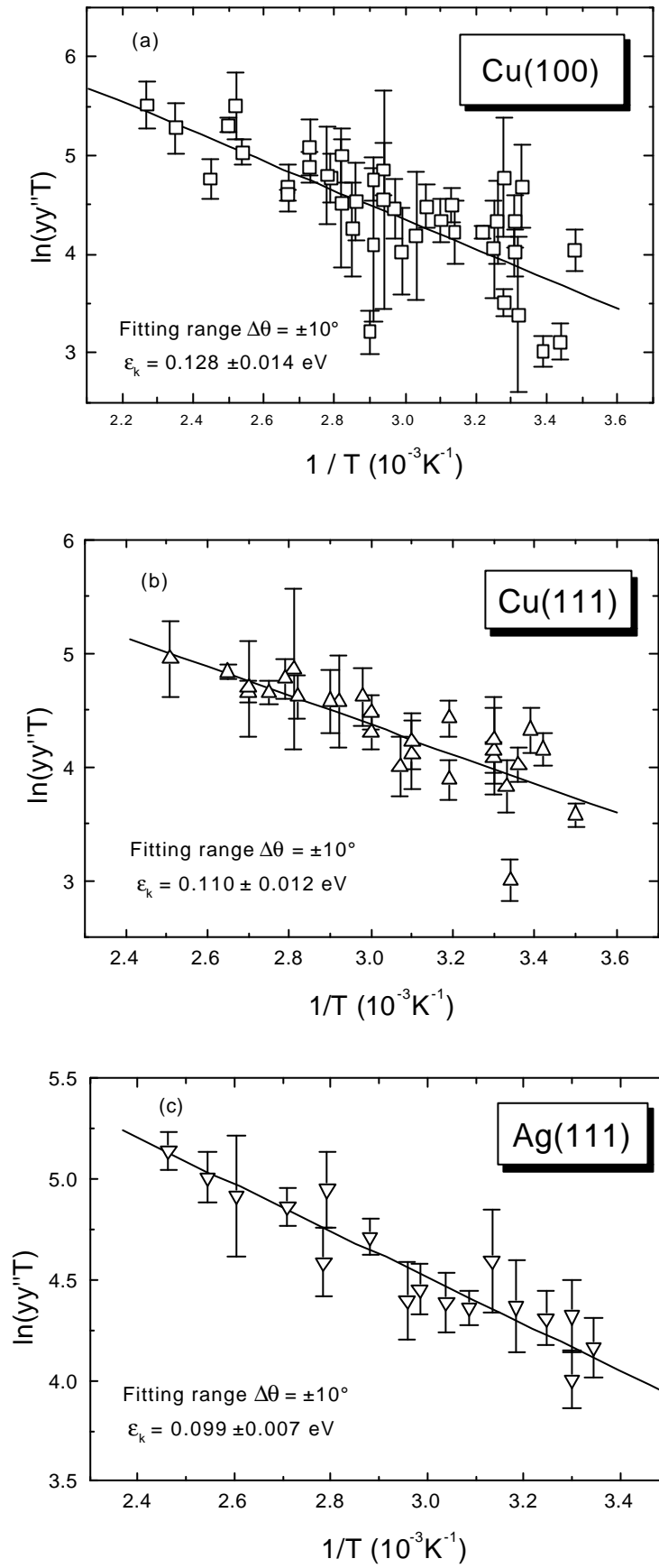
Fig. 13: Arrhenius plots of y y" T for Cu(100), Cu(111) and Ag(111). The curvature y" was obtained by fitting a parabola to the data points between θ = ±10°.
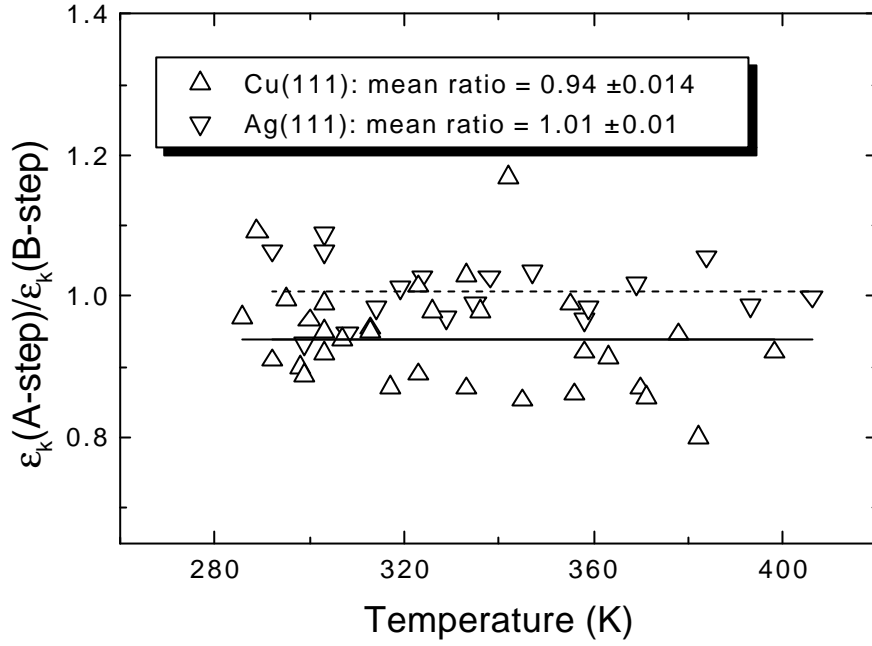
Fig. 14: Ratio of kink energies for A- and B-steps on Cu(111) and Ag(111)

The result is plotted in Fig. 14 for Cu(111) and Ag(111). For Ag(111), the ratio is 1.0 within the error, consistent with the nearly equal step energies for the A- and B-steps (*see also the discussion in section 3 on the possibility of faulted islands*). For Cu(111), the ratio 0.94±0.014 deviates from 1.0 and the deviation is outside the error. With the mean kink energy being 0.117 eV, the kink energies for Cu(111) in A- and B-steps become

$$\varepsilon_k(A) = 0.113 \pm 0.007 \text{ eV}, \quad \varepsilon_k(B) = 0.121 \pm 0.007 \text{ eV}. \tag{40}$$

We note that the error bars concern mainly the absolute value. The ratio of the two kink energies is accurate to about 1.5%.

7.4 Analysis of the aspect ratio

The measured aspect ratios (Fig. 5) are analyzed with the help of eqs. (36) and (37). For Cu(111) and Ag(111), the corrected mean kink energies from Table 2 were used, while for Cu(100), we

have inserted the more accurate value ($\varepsilon_k = 0.128 \pm 0.003$ eV) obtained from the analysis of spatial

step fluctuations [56]. The fits to the experimental data in Fig. 5 were performed leaving the three

parameters in eqs. (36, 37) $\beta(0,0)$, $\beta(\theta_k,0)$ and ΔE_b open. In all cases, the optimum fit was obtained

with $\Delta E_b = 0$. The full lines in Fig. 5 represent the optimum fits. The energies per atom of the straight

step at T = 0 K, $a_\parallel \beta(0,0)$, and the ratios of the step energies of the 100% kinked step to the straight

step $\beta(\theta_k,0) / \beta(0,0)$ are listed in Table 3.

Surface	$a_\parallel \beta$ (eV)	$\beta(\theta_k)/\beta(0°)$ (eV)
Cu(100)	0.22±0.02	1.24±0.01
Cu(111)	0.27±0.03	1.138±0.008
Ag(111)	0.25±0.03	1.136±0.009

Table 3: Step energies per atom $a_\parallel \beta(T=0)$ and ratio of step energies for the 100% kinked step to the energies of the straight step. The error quoted is the sum of the errors obtained by fitting the aspect ratio with ΔE_b set to zero and the error in the determination of the kink energies (Table 2). For Cu(111) the value is lower by 0.04 eV compared to the value published previously in [45]. In that first publication concerning the new method, the data set was restricted to a smaller temperature range.

The errors in Table 3 are the errors obtained from a two parameter fit with ΔE_b set to zero with the

additional error arising from the uncertainty in the determination of the kink energies added.

8. Discussion

In this final section, we discuss the usefulness of the various proposed methods for the analysis of the

equilibrium shapes and compare the numerical result to other experiments as well as to theory. We

begin with the analysis using the Ising-model. As shown in section 7.2, the Ising-model works quite

well for the (111)-surfaces and the Ising parameters obtained from analyzing the equilibrium shapes

agree with the kink energies, experimental errors taken into account. The reason for this good

agreement is twofold. Firstly, for the hexagonal Ising-model, the step energy per atom is twice the

kink energy which is in very good agreement with the experimental values (Table 2 and 3). Secondly, islands in the Ising-model have an aspect ratio of $2/\sqrt{3} = 1.155$ at $T = 0$, which is again very close to the experimental results on Cu(111) and Ag(111) (Table 3). The Ising-model is therefore useful for at least a semi-quantitative analysis of island shapes in cases where merely a less complete set of data is available. An example is the case of islands on Ag(111)-surface in contact with an electrolyte [57]. On (100)-surfaces on the other hand, the Ising analysis does not appear to be helpful in general. There, the Ising-model postulates a ratio of 1 between the kink and the step energy per atom, which is far from reality (Table 2 and 3). Likewise is the aspect ratio at $T = 0$ ill represented by the Ising-model.

As shown in sections 5 and 7.3, kink energies can be determined from an Arrhenius plot of the minimum curvature ("MC-method"). The method competes with the determination of the kink energy from the spatial correlation between pairs of steps on vicinal surfaces [31, 56, 58] ("SC-method"). As discussed in section 7.2, for Cu(100) the results obtained by the two methods agree within the limits of error. The method introduced here requires a larger and also a very accurate data set in a wide temperature range. We have seen furthermore that it is difficult to obtain experimental data on the true minimum curvature and great care has to be exercised in the analysis. The results are nevertheless inevitably less accurate than those obtained with the SC-method. Insofar, the SC-method is first choice. Under certain, not so infrequently encountered circumstances, however, the MC-method has specific advantages. On the Cu(111)-surface, e. g., vicinal surfaces with B-steps are unstable [44]. Furthermore, the step correlation function may be dominated by the time fluctuations of the steps. The condition that the steps are in equilibrium on the one hand while the motion of kinks is slow enough, on the other, is met (if at all) only in a very narrow temperature window [31, 56]. For Cu(111) and Ag(111), this window must be below 300 K (if it does exist at all). A previous analysis of the step correlation function on Ag(111) at 300 K [59] did not take into

account that at 300 K the step position correlation function is dominated by the time structure and the value for the kink energy obtained in this study (0.073 eV) is therefore too low.

The kink energies obtained with the method proposed here agree reasonably well with theory. Here, we focus on the comparison to a recent first principles (GGA) study on Cu(111) steps by Feibelman [60]. For a comparison to the results of other, non first principles methods see [61]. For Cu(111), Feibelman finds energies of 0.092 and 0.117 eV for kinks in the A- and B-steps, respectively. The mean value is about 11% lower than the experimental mean value of 0.117 eV which is outside our estimated experimental error, but not enough outside the error to state a disagreement. Theory and experiment agree in that the energy of the kinks in the A-steps are smaller. What disagrees is the ratio of kink energies $\varepsilon_A/\varepsilon_B$ for which theory finds 0.79 to be compared to the experimental value of 0.94±0.014. As for the step energies, the calculated absolute value for the step energy per atom 0.27 eV for the A-step and 0.26 eV for the B-step [60] is in perfect agreement with our present experiment. Whereas theory calculates the energy of the A-step 4% higher than the energy of the B-step, the experiment has the difference at 1%. Both, theory and experiments are internally consistent insofar as the steps with the higher energies have kinks (which constitute a segment of the other type of step) with the lower energies, and vice versa. Using the "awning approximation" Nelson et al. derived certain relations between kink and step energies [62]. In a recent publication Feibelman [63] extended these considerations to include "corner energies". Under the assumption that corner energies are equal for kinks in A- and B-steps (or vanish all together, whereby the model becomes equivalent to the "awning approximation") the difference in the energies of the A- and the B-step are 2/3 of the difference between the kink energies in the B- and the A-step. Considering the errors, this relation is fulfilled, both by theory and experiment.

The step energy for Cu(111) has also been determined experimentally from the shape fluctuations of islands [32]. A step (free) energy per atom of $a_\| \beta = 0.22 \pm 0.02$ eV was found. This number represents the <u>angle averaged</u> step <u>free</u> energy at the temperature of measurement (around 330 K). According to Fig. 6b, averaging over all angles makes the step free energy about 3.5% higher than the free energy of the densely packed step. Thus, the value quoted should be an upper bound as stated in [32]. The difference is however marginal. More significant for the comparison to the number obtained is the fact that the free energy at 330 K is lower than the energy at $T = 0$ (which is determined here) due to the contribution of phonons. According to [46, 48, 64], the phonon contribution to the step free energy is about 0.01 eV and would therefore do little more than compensating the contribution from averaging over the angle. The value derived from the island fluctuations is thus definitely lower than the value obtained here although the difference is not outside the sum of the errors in both experiments.

Acknowledgement

References

[1]   G. Wulff, Z. Kristallogr. Mineral. 34 (1901) 449.

[2]   W. K. Burton, N. Cabrera, F. C. Frank, Philosophical Transactions Royal Society London Ser. A243 (1951) 299.

[3]   C. Rottman, M. Wortis, Phys. Rev. B24 (1981) 6274.

[4]   C. Jayaprakash, C. Rottman, W. F. Saam, Phys. Rev. B30 (1984) 6549.

[5]   C. Jayaprakash, W. F. Saam, Phys. Rev. B30 (1984) 3916.

[6]   C. Rottman, M. Wortis, Phys. Rev. B29 (1984) 328.

[7]   C. Rottman, M. Wortis, Phys. Rep. 103 (1984) 59.

[8]   M. Wortis, in R. Vanselow, R. Howe (Eds.): *Chemistry and Physics of Solid Surfaces, Vol. 7*, Springer, New York 1988, p. 367.

[9]   J. C. Heyraud, J. J. Metois, Acta Met. 28 (1980) 1789.

[10]   J. C. Heyraud, J. J. Metois, Surf. Sci. 177 (1986) 213.

[11]   J. C. Heyraud, J. J. Metois, Surf. Sci. 128 (1983) 334.

[12]   K. Arenhold, S. Surnev, P. Coenen, H. P. Bonzel, P. Wynblatt, Surf. Sci. 417 (1998) L1160.

[13]   K. Arenhold, S. Surnev, H. P. Bonzel, P. Wynblatt, Surf. Sci. 424 (1999) 271.

[14]   J. M. Bermond, J. J. Métois, X. Egéa, F. Floret, Surf. Sci. 330 (1995) 48.

[15]   J. M. Bermond, J. J. Métois, J. C. Heyraud, F. Floret, Surf. Sci. 416 (1998) 430.

[16]   S. Surnev, K. Arenhold, P. Coenen, B. Voigtländer, H. P. Bonzel, Journal of Vacuum Science and Technology A 16 (1998) 1059.

[17]   J. Frohn, M. Giesen, M. Poensgen, J. F. Wolf, H. Ibach, Phys. Rev. Lett. 67 (1991) 3543.

[18]   N. C. Bartelt, J. L. Goldberg, T. L. Einstein, E. D. Williams, Surf. Sci. 273 (1992) 252.

[19]   M. Giesen, G. S. Icking-Konert, Surface Review and Letters 6 (1999) 27.

[20]   M. Giesen, T. L. Einstein, Surf. Sci. 449 (2000) 191.

[21]   N. C. Bartelt, T. L. Einstein, E. D. Williams, Surf. Sci. 240 (1990) L591.

[22]   V. I. Marchenko, A. Y. Parshin, Sov. Phys. JETP 52 (1981) 129.

[23]   J. W. M. Frenken, P. Stoltze, Phys. Rev. Lett. 82 (1999) 3500.

[24]   N. Garcia, P. A. Serena, Surf. Sci. 330 (1995) L665.

[25]   E. L. Goff, L. Barbier, L. Masson, B. Salanon, Surf. Sci. 432 (1999) 139.

[26]   A. Pavlovska, K. Faulian, E. Bauer, Surf. Sci. 221 (1989) 233.

[27]   H. P. Bonzel, A. Emundts, Phys. Rev. Lett. 84 (2000) 5804.

[28]   B. S. Swartzentruber, Y.-W. Mo, R. Kariotis, M. G. Lagally, M. B. Webb, Phys. Rev. Lett. 65 (1990) 1913.

[29]   E. D. Williams, R. J. Phaneuf, J. Wei, N. C. Bartelt, T. L. Einstein, Surf. Sci. 294 (1993) 219.

[30]   M. Giesen-Seibert, F. Schmitz, R. Jentjens, H. Ibach, Surf. Sci. 329 (1995) 47.

[31]   M. Giesen, G. S. Icking-Konert, D. Stapel, H. Ibach, Surf. Sci. 366 (1996) 229.

[32]   D. C. Schlößer, L. K. Verheij, G. Rosenfeld, G. Comsa, Phys. Rev. Lett. 82 (1999) 3843.

[33]   N. C. Bartelt, R. M. Tromp, E. D. Williams, Phys. Rev. Lett. 73 (1994) 1656.

[34]   T. Michely, G. Comsa, Surf. Sci. 256 (1991) 217.

[35]   K. Morgenstern, G. Rosenfeld, G. Comsa, Phys. Rev. Lett. 76 (1996) 2113.

[36]   K. Morgenstern, G. Rosenfeld, E. Laegsgaard, F. Besenbacher, G. Comsa, Phys. Rev. Lett. 80 (1998) 556.

[37]   J. Frohn, J. F. Wolf, K. Besocke, M. Teske, Rev. Sci. Instrum. 60 (1989) 1200.

[38]   K. Besocke, Surf. Sci. 181 (1987) 145.

[39]   M. Giesen, G. S. Icking-Konert, Surf. Sci. 412/413 (1998) 645.

[40]   M. Giesen, C. Steimer, H. Ibach, (to be published) .

[41]   G. Schulze-Icking-Konert, PhD Thesis, University of Aachen D82, Jül-Report 3588, Forschungszentrum Jülich (1998) .

[42]   K. Meinel, M. Klaua, H. Bethge, phys. stat. sol. 110 (1988) 189.

[43]   J. Camarero, J. d. l. Figuera, J. J. d. Miguel, R. Miranda, J. Àlvarez, S. Ferrer, Surf. Sci. 459 (2000) 191.

[44]   M. Giesen, U. Linke, H. Ibach, Surf. Sci. 389 (1997) 264.

[45]   G. Schulze-Icking-Konert, M. Giesen, H. Ibach, Phys. Rev. Lett. 83 (1999) 3880.

[46]   A. Kara, S. Durukanoglu, T. S. Rahman, Phys. Rev. B 53 (1996) 15489.

[47]   A. Kara, S. Durukanoglu, T. S. Rahman, J. Chem. Phys 106 (1997) 2031.

[48]   S. Durukanoglu, A. Kara, T. S. Rahman, (to be published) .

[49]   R. K. P. Zia, J. E. Avron, Phys. Rev. B25 (1982) 2042.

[50]   R. K. P. Zia, J. Stat. Phys. 45 (1986) 801.

[51]   C. Herring, in R. Gomer (Ed.): *Structure and Properties of Solid Surfaces*, The University of Chicago Press, Chicago 1953, p. 5.

[52]   M. C. Desjonqueres, D. Spanjaard, *Concepts in surface physics*, Springer, Berlin, Heidelberg, New York 1996.

[53]   N. C. Bartelt, T. L. Einstein, E. D. Williams, Surf. Sci. 276 (1992) 308.

[54]   W. Feller, *An Introduction to Probability Theory and Its Applications, Vol. I*, Wiley, New York 1968.

[55]   L. Verheij, private commun. .

[56]   M. Giesen-Seibert, H. Ibach, Surf. Sci. 316 (1994) 205.

[57]   M. Giesen, R. Randler, S. Baier, H. Ibach, D. M. Kolb, Electrochim. Acta 45 (1999) 527.

[58]   M. F. Chang, M. S. Hoogeman, M. A. J. Klik, J. W. M. Frenken, Surf. Sci. 432 (1999) 21.

[59]   M. Poensgen, J. F. Wolf, J. Frohn, M. Giesen, H. Ibach, Surf. Sci. 274 (1992) 430.

[60]   P. Feibelman, Phys. Rev. B 60 (1999) 11118.

[61]   M. Giesen, Prog. Surf. Sci. in press (2000) .

[62]   R. C. Nelson, T. L. Einstein, S. V. Khare, P. J. Rous, Surf. Sci. 295 (1993) 462.

[63]   P. Feibelman, Surf. Sci. in press (2000) .

[64]   A. Kara, P. Staikov, T. S. Rahman, Phys. Rev. B61 (2000) 5714.